Correction published 19 September 2006

Reconstruction of sea surface temperature variations in the Arabian Sea over the last 23 kyr using organic proxies (TEX_{86} and $U^{K'}_{37}$)

Carme Huguet,[1] Jung-Hyun Kim,[2,3] Jaap S. Sinninghe Damsté,[1] and Stefan Schouten[1]

Received 6 September 2005; revised 13 February 2006; accepted 27 March 2006; published 20 July 2006.

[1] Two sediment cores from the western Arabian Sea, NIOP905 and 74KL, were analyzed to determine sea surface temperature (SST) variations over the last 23 kyr. Two organic molecular SST proxies were used, the well-established $U^{K'}_{37}$ based on long-chain unsaturated ketones synthesized by haptophyte algae and the newly proposed TEX_{86} derived from the membrane lipids of Crenarchaeota. Comparison of NIOP905 and 74KL core top data with present-day SST (0–10 m) values indicates that both proxies yield temperatures similar to local annual mean SSTs. However, TEX_{86} and $U^{K'}_{37}$ SST down-core records derived from the same cores differ in magnitude and phasing. The alkenone SST record of NIOP905 shows small changes in SST (~0.5°C) over the last 23 kyr, while that of core 74KL shows a ~2°C increase from the Last Glacial Maximum (LGM) (23–19 calendar (cal) kyr B.P.) through the Holocene (the last 11.5 cal kyr B.P.) synchronous with changes in the Northern Hemisphere. In contrast, the TEX_{86} records of both cores show a large increase in SST from 22°–23°C in the LGM to 28°–30°C during Termination I (19–11.5 cal kyr B.P.), decreasing to present-day annual means of ~26°C. A cold phase between 14.5 and 12 cal kyr B.P. that may correspond to the Antarctic cold reversal is also observed. This implies a Southern Hemisphere control on tropical SST reconstructed by the TEX_{86}, possibly related to SW monsoon. Our results suggest that the application of both TEX_{86} and $U^{K'}_{37}$ give different but complementary information on SST developments in past marine environments.

Citation: Huguet, C., J.-H. Kim, J. S. S. Damsté, and S. Schouten (2006), Reconstruction of sea surface temperature variations in the Arabian Sea over the last 23 kyr using organic proxies (TEX_{86} and $U^{K'}_{37}$), *Paleoceanography*, *21*, PA3003, doi:10.1029/2005PA001215.

1. Introduction

[2] Evidence of large-magnitude and rapid climate changes on millennial timescales (e.g., Dansgaard-Oeschger events, Heinrich Events) that characterized the last glaciation during the Late Pleistocene have been provided by ice core records [e.g., *Grootes and Stuiver*, 1997; *Jouzel et al.*, 2003] as well as by continental and marine sediment records [e.g., *Schulz et al.*, 1998; *Wang et al.*, 2001]. To better understand such abrupt millennial-scale climate changes, their consequences, and their underlying mechanisms, it is essential to construct SST records at a high temporal resolution.

[3] Several geochemical proxies are used for SST reconstruction, the most common being $\delta^{18}O$ and Mg/Ca ratios of planktic foraminifera [*Chave*, 1954; *Emiliani*, 1955; *Nurnberg et al.*, 1996] and the $U^{K'}_{37}$ index of long-chain unsaturated ketones synthesized by haptophyte algae [*Brassell et al.*, 1986]. Reconstruction of SST with these proxies is, however, associated with a number of problems. The use of planktic foraminifera $\delta^{18}O$ for SST reconstruction is complicated by several uncertainties related to the formation and preservation of shells as well as the carbonate ion concentration, the $\delta^{18}O$ and the salinity of the original seawater [*Spero et al.*, 1997; *Wefer et al.*, 1999; *Lea*, 2003]. The Mg/Ca ratio [*Elderfield and Ganssen*, 2000] is less affected by these factors, except by species-dependent vital effects and shell dissolution [*Wefer et al.*, 1999; *Lea*, 2003]. The $U^{K'}_{37}$ index is often considered more robust, as the values are not directly controlled by seawater chemistry, and hence assumptions concerning this are not needed. Furthermore, global surveys of surface sediments and particulate organic matter reveal a strong and identical correlation between the $U^{K'}_{37}$ and SST (reviewed by *Herbert* [2003]). However, the biochemical function of alkenones is still unknown and the $U^{K'}_{37}$ may be affected by changes in the species composition through time and also by oxic degradation [*Herbert*, 2003].

[4] Recently, *Schouten et al.* [2002] introduced a new SST proxy, the TEX_{86} based on the relative distribution of glycerol dibiphytanyl glycerol tetraethers (GDGTs), which are membrane lipids produced by nonthermophilic Crenarchaeota. These organisms are ubiquitous and abundant in seawater [*Hoefs et al.*, 1997; *Massana et al.*, 2000; *Karner et al.*, 2001] and large lakes [*Powers et al.*, 2005]. Marine crenarchaeota biosynthesize different GDGTs with a varying number of cyclopentane rings according to temperature [*Wuchter et al.*, 2004]. Therefore, by measuring the relative amounts of GDGTs present in sediments, the temperature at which Crenarchaeota were living can be reconstructed. Experiments with an enrichment culture, containing a single

[1]Department of Marine Biogeochemistry and Toxicology, Royal Netherlands Institute for Sea Research, Texel, Netherlands.
[2]Fachbereich 5 Geowissenschaften, University of Bremen, Bremen, Germany.
[3]Now at Centre de Formation et de Recherche sur l'Environnement Marin-CNRS UMR 5110, Université de Perpignan, Perpignan, France.

Copyright 2006 by the American Geophysical Union.
0883-8305/06/2005PA001215

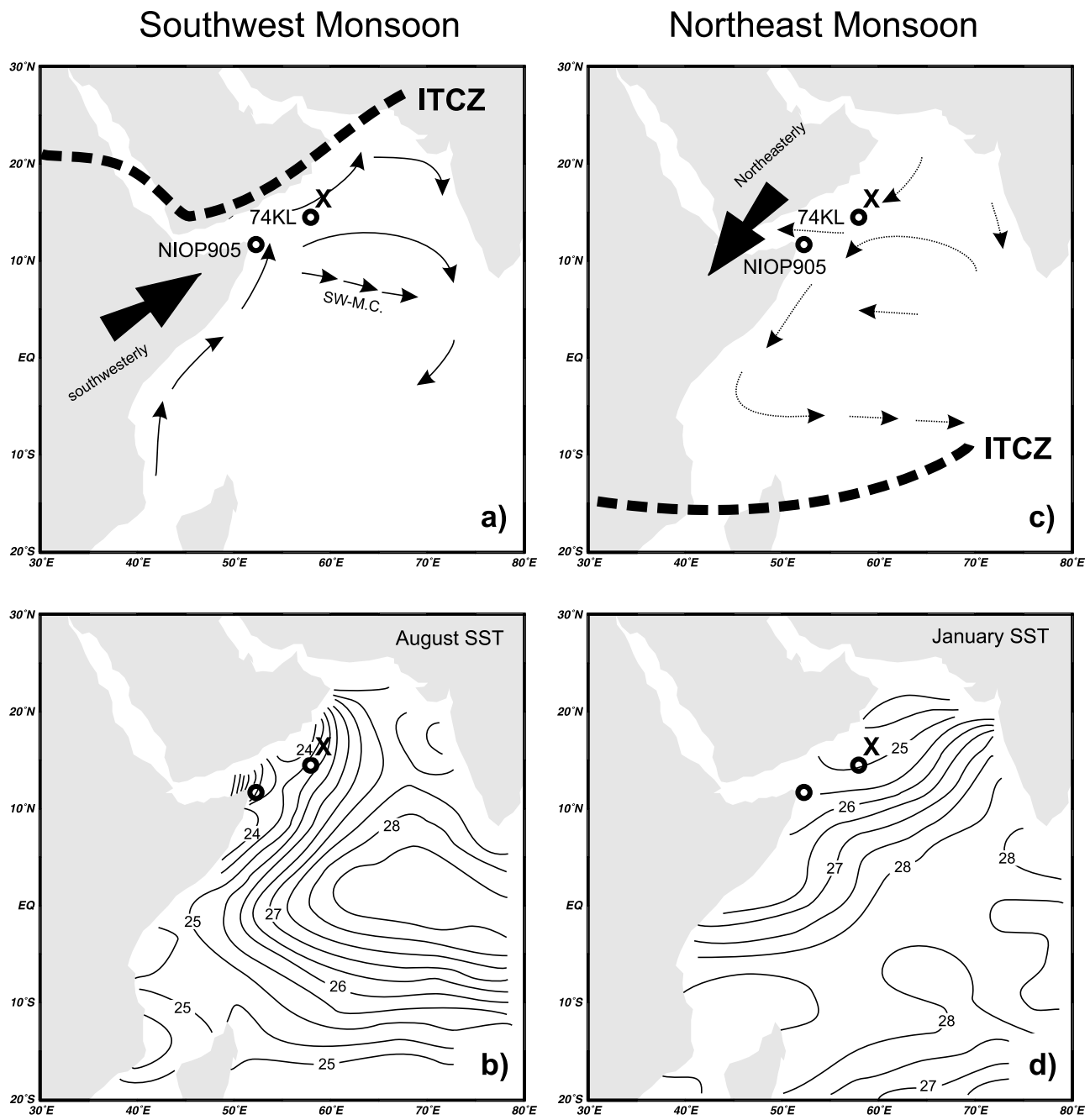

Figure 1. Map of study area showing core locations (circles), sediment trap location of *Wakeham et al.* [2002] and C. Wuchter et al. (submitted manuscript, 2006) (cross), Intertropical Convergence Zone (ITCZ) positions, and prevalent wind directions during the SW monsoon and the NE monsoon. (a) Sea surface circulation pattern during the SW monsoon. (b) August sea surface temperature (SST) distribution pattern [*Levitus and Boyer*, 1994]. (c) Sea surface circulation pattern during the NE monsoon. (d) January SST distribution pattern [*Levitus and Boyer*, 1994]. Core NIOP905 (10°47′N, 51°56′E) was taken in the Somalia Basin, under the Socotra upwelling. Core 74 KL (14°19.26′N, 57°20.82′E) was taken off the Oman coast.

archaeal species falling in the phylogenetic cluster of the marine crenarchaeota, showed that TEX_{86} is linearly correlated with temperature and that changes in salinity and nutrients do not substantially affect the TEX_{86} [*Wuchter et al.*, 2004]. Particulate organic matter analysis revealed that the TEX_{86} correlates well with surface water temperatures (depths < 100m) and that the signal in the deeper water layers and surface sediments is primarily derived from these upper 100 meters [*Wuchter et al.*, 2005]. This suggests that the signal from the surface waters is efficiently transported

to the sediment probably by grazing [*Wakeham et al.*, 2003]. Indeed, recent studies of sediment trap material showed that the TEX_{86} signal at different depths in sediment particles is derived from the upper layer of the water column (C. Wuchter et al., Archaeal tetraether membrane lipid fluxes in the northeastern Pacific and Arabian sea: Implications for TEX_{86} paleothermometry, submitted to *Paleoceanography*, 2006, hereinafter referred to as Wuchter et al., submitted manuscript, 2006). This new organic geochemical proxy also seems to be unaffected by water redox conditions [*Schouten et al.*, 2004]. However, a number of factors such as the ecology and physiology of crenarchaeota in different oceanic provinces and its effect on the TEX_{86}, need to be further constrained. However, there are already some developments in those fields, for example, a species of marine Crenarchaeota was recently isolated and shown to be an autotrophic ammonium oxidizer [*Konekes et al.*, 2005] in agreement with previous observations [*Wuchter et al.*, 2004]. This could explain observed seasonal distributions of marine Crenarchaeota in surface waters, i.e., their high abundance during times of low phytoplankton productivity and high nutrients [cf. *Wuchter et al.*, 2005, and references therein]. However, to what extent this influences their depth habitat, their seasonality in low- and high-nutrient environments and how widespread this metabolism is remains unknown. Recently, it has also become clear that GDGTs such as those occurring in marine Crenarchaeota are present in terrestrial organic matter albeit in much lower abundances [*Hopmans et al.*, 2004; *Weijers et al.*, 2004]. Thus, at sites which receive high amounts of terrestrial organic matter, the TEX_{86} could potentially be biased. Nevertheless, despite these limitations, the TEX_{86} proxy may be a useful tool to reconstruct SSTs.

[5] Here, for the first time, we applied the TEX_{86} to Quaternary marine sediment cores and investigated its potential as a tool in multi proxy paleoceanography and paleoclimate studies in comparison with the $U^{K'}_{37}$. The western Arabian Sea (Figure 1) was selected for this study as it is an area where organic-rich sediments are deposited with high accumulation rates, allowing the recovery of continuous high-resolution records with sufficient amounts of organic matter. Furthermore, previous low-resolution $U^{K'}_{37}$ records from this area revealed quite contrasting differences between LGM and Holocene SSTs varying between 0.3°C and 3°C [*Sonzogni et al.*, 1998]. Our approach based on two lipid biomarker proxies, $U^{K'}_{37}$ and TEX_{86}, provides detailed information on SST variations in the western Arabian Sea over the last 23 kyr and the impact of the Arabian Sea monsoonal climate system on SST records.

2. Material and Methods

2.1. Modern Atmospheric and Oceanographic Setting

[6] The western Arabian Sea is predominantly influenced by monsoon climate related annual cycles driven by the pressure gradient that exists between the Tibet plateau and the South Indian Ocean [*Rixen et al.*, 2000]. The annual cycle can be divided into four phases: (1) the northeast (NE) monsoon from December to March; (2) the summer intermonsoon from March to June; (3) the southwest (SW) monsoon from June to September; and (4) the fall intermonsoon from September to December [*Wakeham et al.*, 2002]. The differential pressure results in southwesterly winds during the SW monsoon and in northeasterly winds during the NE monsoon [*Rixen et al.*, 2000; *Andruleit et al.*, 2000; *Bush*, 2002]. The SW monsoon induces strong upwelling of nutrient rich, cool waters that leads to lower SST (Figure 1), higher productivity, an intense oxygen minimum zone and a high particle flux [*Wakeham et al.*, 2002]. The NE monsoon causes a deepening of the mixed layer and no upwelling, resulting in relatively higher SST (Figure 1) and only a small increase in production and particle flux [*Wakeham et al.*, 2002].

2.2. Sample Collection and Stratigraphy

[7] Two sediment cores (NIOP905 and 74KL) from the western Arabian Sea were investigated in this study. Core NIOP905 (10°47′N, 51°56′E) was taken in the Socotra upwelling cell of the Somalia Basin (Figure 1), approximately 80 km off the coast of Somalia and at 1567 m water depth. Core 74KL (14°19′N, 57°20′E) was obtained from the East Sheba Ridge, 1000 m above the turbidity plain of the Indus fan, 300 km south of the Arabian continental margin (Figure 1). Core NIOP905 was sampled at 2 to 5 cm intervals and core 74KL at 2.5 cm intervals. Both cores have been studied previously in detail for the $\delta^{18}O$ of foraminifera [*Sirocko et al.*, 1993; *Ivanova*, 1999; *Jung et al.*, 2002; *Ivanochko et al.*, 2005] and, in case of NIOP905, trace elements [*Ivanochko et al.*, 2005].

[8] The age models of cores NIOP905 and 74KL were established by nineteen accelerator mass spectrometry (AMS) ^{14}C dates from mixed planktic foraminifera and thirteen AMS ^{14}C determinations on *Globigerinoides ruber*, respectively (Table 1) which were published previously [*Sirocko et al.*, 1993; *Ivanova*, 1999; *Jung et al.*, 2002; *Ivanochko et al.*, 2005]. We employed a correction for the regional ^{14}C reservoir age (ΔR = the deviation from the surface ocean average of 400 years) of 190 ± 25 years for the western Arabian Sea [*Southon et al.*, 2002], although the ΔR in the Arabian Sea can vary substantially through time as demonstrated by *Staubwasser et al.* [2002]. However, the age model based on the varying ΔR of *Staubwasser et al.* [2002] from the eastern Arabian Sea (not shown) does not affect the conclusions made in this study. Continuous timescales for both cores were obtained by linear interpolations between the age control points after converting the ^{14}C ages into calendar years (years before 1950) using the latest version of the radiocarbon calendar year calibration software CALIB 5.0.1 (M. Stuiver et al., available at http://calib.qub.ac.uk/calib/, 2005). The average temporal resolution is ~200 years for NIOP905 and ~300 years for core 74KL.

2.3. Lipid Extraction

[9] For core NIOP905, freeze-dried and homogenized sediment samples were ultrasonically extracted with MeOH, MeOH/DCM (1:1;v/v) and finally with DCM. The supernatants were collected and after evaporating the solvents, the extracts were dried over a sodium sulfate column. An aliquot of the total lipid extract was used to analyze the

Table 1. Age Control Points for Sediment Cores NIOP905 and 74KL

Sediment Core/Depth in Core, cm	Uncorrected AMS ^{14}C Ages, years B.P.	Analytical Error (±1-σ),[a] years	ΔR,[b] years	ΔR Error, years	Calibrated Calendar Ages (2-σ ranges), cal years B.P.	Calibrated Calendar Ages (1-σ ranges), cal years B.P.	Mean Calibrated Calendar Ages Used for the Age Models, cal years B.P.	Reference for Original AMS ^{14}C Data
NIOP 905								
20	1410	NA	190	±25	664–890	691–820	755.5	*Ivanova* [1999]
40	2420	NA	190	±25	1692–1972	1760–1905	1832.5	*Ivanova* [1999]
80	4050	NA	190	±25	3656–3977	3728–3894	3811.0	*Ivanova* [1999]
120	5410	NA	190	±25	5458–5703	5520–5645	5582.5	*Ivanova* [1999]
167–167.5[c]	6653	50	190	±25	6812–7135	6874–7042	6958.0	*Jung et al.* [2002]
183–183.5[c]	7125	50	190	±25	7332–7552	7398–7501	7449.5	*Jung et al.* [2002]
200	7620	45	190	±25	7776–7997	7839–7944	7891.5	*Ivanova* [1999]
249.5–251[c]	8620	50	190	±25	8892–9240	8972–9117	9044.5	*Jung et al.* [2002]
291–291.5[c]	9748	50	190	±25	10261–10538	10355–10505	10430.0	*Jung et al.* [2002]
313.75	10371	47	190	±25	11101–11256	11146–11214	11180.0	*Ivanochko* [2005]
320	10500	NA	190	±25	11174–11433	11210–11346	11278.0	*Ivanova* [1999]
340	11100	NA	190	±25	12236–12709	12434–12632	12533.0	*Ivanova* [1999]
360	12000	NA	190	±25	13162–13383	13215–13314	13264.5	*Ivanova* [1999]
361.25	12131	62	190	±25	13247–13556	13297–13431	13364.0	*Ivanochko* [2005]
376.25	12895	52	190	±25	14002–14602	14044–14287	14165.5	*Ivanochko* [2005]
391.25	13975	55	190	±25	15518–6300	15688–16067	15877.5	*Ivanochko* [2005]
400	14190	NA	190	±25	15811–16593	15978–16366	16172.0	*Ivanova* [1999]
411.25	14701	61	190	±25	16385–17197	16620–17029	16824.5	*Ivanochko* [2005]
480.25	20580	114	190	±25	23598–24298	23778–24109	23943.5	*Ivanochko* [2005]
74KL								
7.5	1230	60	190	±25	509–711	553–656	604.5	*Sirocko et al.* [1993]
35	3350	100	190	±25	2736–3229	2825–3096	2960.5	*Sirocko et al.* [1993]
55	5540	90	190	±25	5539–5922	5623–5832	5727.5	*Sirocko et al.* [1993]
70	7850	90	190	±25	7941–8320	8004–8213	8108.5	*Sirocko et al.* [1993]
80	8700	120	190	±25	8831–9440	8989–9298	9143.5	*Sirocko et al.* [1993]
97.5	10580	120	190	±25	11177–11927	11245–11670	11457.5	*Sirocko et al.* [1993]
115	11780	130	190	±25	12881–13285	12962–13189	13075.5	*Sirocko et al.* [1993]
127.5	13060	150	190	±25	14049–15064	14220–14816	14518.0	*Sirocko et al.* [1993]
142.5	14200	170	190	±25	15617–16763	15889–16471	16180.0	*Sirocko et al.* [1993]
160	15880	170	190	±25	18096–18896	18501–18855	18678.0	*Sirocko et al.* [1993]
165	16260	170	190	±25	18668–19244	18781–19033	18907.0	*Sirocko et al.* [1993]
180	17130	180	190	±25	19344–20072	19509–19846	19677.5	*Sirocko et al.* [1993]
197.5	20580	260	190	±25	22990–24594	23590–24288	23939.0	*Sirocko et al.* [1993]

[a]NA indicates that analytical errors are not available for these data. Therefore we assumed ±50 years for the analytical determination.
[b]The regional reservoir age (ΔR) for the western Arabian Sea was used according to *Southon et al.* [2002].
[c]Mean values were used for the age model.

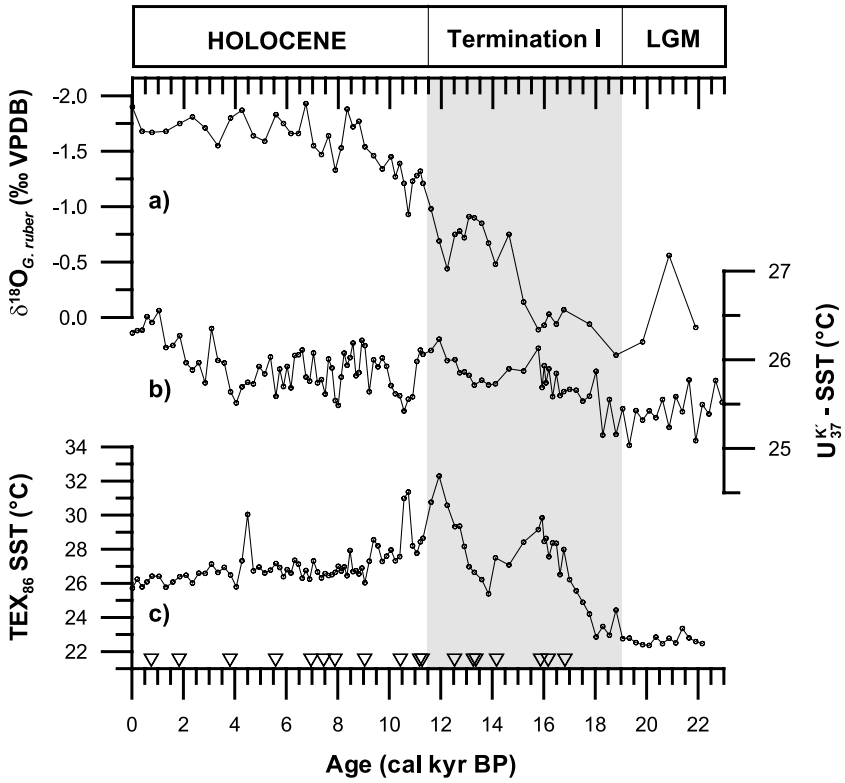

Figure 2. Time series of (a) stable $\delta^{18}O$ record of the planktic foraminifera *G. ruber* [from *Jung et al.*, 2001] and (b) $U^{K'}_{37}$ and (c) TEX_{86} SST records for core NIOP905, plotted against calendar ages. Triangles on lower axis show age control points. Broad shaded bar indicates the time interval for Termination I.

alkenones for determination of the $U^{K'}_{37}$ ratio. The total extract was derivatized with diazomethane and BSTFA/pyridine. The derivatized total extract was analyzed by gas chromatography (GC) and gas chromatography/mass spectrometry to quantify alkenones. For GDGT analysis an aliquot of the total lipid extract was divided into apolar and polar fractions using a small column with activated alumina and using hexane/DCM (9:1;v/v) and DCM/MeOH (1:1;v/v) as eluents, respectively. The polar fractions were analyzed for GDGTs.

[10] For core 74KL, the samples were extracted in a similar way than NIOP905. Subsequently, the total extracts were separated into DCM and MeOH/DCM (1:1;v/v) fractions, using a silica gel cartridge (Varian Bond Elute; 1 cc per 100 mg). The DCM fraction was saponified at 80°C for 2 h with 300 μl of 0.1 M KOH in 90:10 MeOH/H_2O. The neutral fraction containing the alkenones was obtained by partitioning into hexane. The MeOH/DCM (1:1;v/v) fraction was used for GDGT analysis.

2.4. Alkenone Analysis and $U^{K'}_{37}$ SST

[11] Peak areas of $C_{37:2}$ and $C_{37:3}$ alkenones were determined by GC analysis [cf. *Kim et al.*, 2002]. The alkenone unsaturation index $U^{K'}_{37}$ was calculated from $U^{K'}_{37} = (C_{37:2})/(C_{37:2} + C_{37:3})$, where $C_{37:2}$ and $C_{37:3}$ are the di- and tri-unsaturated C_{37} methyl alkenones [*Prahl and Wakeham*, 1987]. The $U^{K'}_{37}$ values were converted into temperature values applying the global core top calibration ($U^{K'}_{37} = 0.033 \times T + 0.044$) of *Müller et al.* [1998].

2.5. GDGT Analysis and TEX_{86} SST

[12] For cores NIOP905 and 74KL, the polar fractions (DCM/MeOH, 1:1; v/v) were analyzed for GDGTs according to the procedure described by *Hopmans et al.* [2000]. Aliquots of polar fractions were blown down under a stream of nitrogen, redissolved in hexane/propanol (99:1;v/v), and filtered through 0.45 μm PTFE filters. The samples were analyzed with an HP (Palo Alto, CA, USA) 1100 series LC-MS equipped with an autoinjector and Chemstation chromatography manager software. Separation was achieved on a Prevail Cyano column (2.1 × 150 mm, 3 μm; Alltech, Deerfield, Illinois, USA), maintained at 30°C. The GDGTs were eluted using a changing mixture of hexane (A) and propanol (B) as follows, 99 A:1 B for 5 min, then a linear gradient to 1.8 B in 45 min. Detection was achieved using atmospheric pressure chemical ionization mass spectrometry of the eluent. Single Ion Monitoring (SIM) was used as it gives better reproducibility than full mass scanning by reducing the signal-to-noise ratio. The SIM method was set to scan the 5 $[M^+]$+H ions of the GDGTs with a dwell time of 237 ms for each ion. All TEX_{86} analyses were performed at least in duplicate.

[13] The TEX_{86} ratio (TEX_{86}= ($GDGT_2$ + $GDGT_3$ + Crenarchaeol-isomer)/($GDGT_1$ + $GDGT_2$ + $GDGT_3$ +

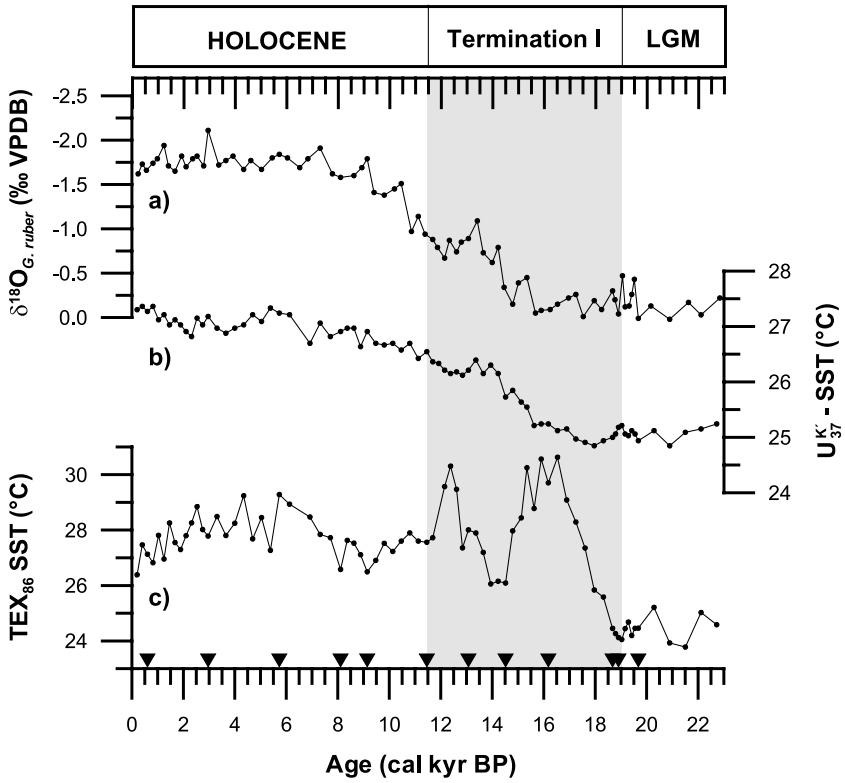

Figure 3. Time series of (a) stable $\delta^{18}O$ record of the planktic foraminifera *G. ruber* [*Sirocko et al.*, 1993] and (b) $U^{K'}_{37}$ and (c) TEX_{86} SST records for core 74KL, plotted against calendar ages. Triangles on lower axis show age control points. Broad shaded bar indicates the time interval for Termination I.

Crenarchaeol-isomer)) was calculated based on the relative abundance of GDGTs and converted into temperature values applying the calibration ($TEX_{86} = 0.015 \times T + 0.028$) of *Schouten et al.* [2002].

2.6. Analytical Reproducibility

[14] To determine the analytical reproducibility of the $U^{K'}_{37}$ and TEX_{86} SST values, a set of 12 subsamples from a large homogenized batch of sediment from GeoB 1707-1 (recovered during METEOR cruise M20/2 at 1232 m near the Angola coast in the Atlantic Ocean; 19°41′S, 10°39′E) were extracted independently and measured at regular intervals during the analysis of the 74KL sample series. The standard deviation of the $U^{K'}_{37}$ and TEX_{86} SST analysis of these subsamples was 0.2°C (±1σ) and 0.4°C (±1σ), respectively.

3. Results

3.1. Core NIOP905

[15] The $U^{K'}_{37}$ SST range for NIOP905 is fairly narrow and varies between 25.0 and 26.5°C for the time interval between 23 and 0 cal kyr B.P. This is in contrast to the $\delta^{18}O$ record of *G. ruber* [*Jung et al.*, 2001] which shows a gradual decrease during Termination I (Figure 2a). $U^{K'}_{37}$ SST during the LGM (23–19 cal kyr B.P.) was 25.5°C with only a small, relatively abrupt increase in SST during the glacial-interglacial transition between 18 to 16 cal kyr B.P. of ~0.5°C (Figure 2b). After this rise, the NIOP905 record shows a small drop in $U^{K'}_{37}$ SST of ~0.5°C between 16 and 14 cal kyr B.P. and a rise of ~0.5°C between 14 and 12.5 cal kyr B.P. This is followed by a decrease of ~0.7°C between 12 and 10.5 cal kyr B.P. Then SST stabilized around 25.7°C until 5 cal kyr B.P. and then rose to the core top value of 26.3°C.

[16] The TEX_{86} record for NIOP905 is quite different from the $U^{K'}_{37}$ SST record and the $\delta^{18}O$ record. TEX_{86} SST values for the studied interval of 23–0 cal kyr B.P. range from 22 to approximately 30°C with a few data points above 30°C (Figure 2c). TEX_{86} SST is ~22.5°C during the LGM (23–19 cal kyr B.P.) and increased to 29°C between 18 and 16 cal kyr B.P. This ~6°C increase is significant compared to the analytical error of 0.4°C. After the rapid warming of SST between 18 and 16 cal kyr B.P. there was a substantial lowering of SST to ~26°C between 16 and 14 cal kyr B.P. (Figure 2c). After this cooling, the TEX_{86} SST increased again by up to 5°C to a maximum of 31°C at 12 cal kyr B.P. before rapid cooling of ~3°C until 11 cal kyr B.P. An additional SST spike of ~3°C is noticeable at around 10.5 cal kyr B.P. and SST then slowly decreased from 27°C at 10 cal kyr B.P. to the present-day core top value of 25.7°C.

3.2. Core 74KL

[17] The $U^{K'}_{37}$ SST range for 74KL is larger than for NIOP905 and varies from 24.8 to 27.3°C between 23 and 0 cal kyr B.P. (Figure 3b). SST during the LGM (23–19 cal kyr B.P.) was again 25°C as with NIOP905 but the increase

Table 2. Mean Monthly Sea Surface Temperature (0–10 m) Data Corresponding to Core Sites [*World Ocean Atlas*, 1998], Calculated Flux Weighted TEX_{86} and $U^{K'}_{37}$ SST, and Core Top TEX_{86} and $U^{K'}_{37}$ SST Values for NIOP905 and 74KL

	Site NIOP905		Site 74KL	
Phase/Month	Monthly Mean Temperature, °C	Seasonal Mean Temperature, °C	Monthly Mean Temperature, °C	Seasonal Mean Temperature, °C
Northeast Monsoon				
December	26.4		26.0	
January	25.9		25.4	
February	25.8	26.0	25.1	25.5
Summer Intermonsoon				
March	26.9		26.7	
April	28.7		28.8	
May	28.6	28.2	29.7	28.4
Southwest Monsoon				
June	26.1		28.7	
July	23.3		25.7	
August	22.7		24.8	
September				
Fall Intermonsoon	23.8	24.0	25.4	26.2
October	26.9		27.5	
November	27.2	27.1	27.2	27.4

	Site NIOP905	Site 74KL
Annual mean	26.0	26.8
Alkenone flux weighted mean[a]	24.6	25.9
GDGT flux weighted mean[b]	26.0	26.8
$U^{K'}_{37}$ core top[c]	25.7	26.6
$U^{K'}_{37}$ core top[d]	25.9	27.3
$U^{K'}_{37}$ core top[e]	26.3	27.3
TEX_{86} core top	25.7	26.4

[a]Calculated using flux data of *Prahl et al.* [2000] and mean monthly SST.
[b]Calculated using flux data of *Wuchter et al.* [2005] and mean monthly SST.
[c]According to the calibration of *Prahl et al.* [1988]: T [°C] = ($U^{K'}_{37}$-0.039)/0.034.
[d]According to the calibration of *Sonzogni et al.* [1997]: T [°C] = ($U^{K'}_{37}$-0.317)/0.023.
[e]According to the calibration of *Müller et al.* [1998]: T [°C] = ($U^{K'}_{37}$-0.033)/0.04.

in SST during Termination I was larger (~1.5°C) and more gradual in 74KL and was synchronous with the decrease in $\delta^{18}O$ values of *G. ruber* (Figures 3a and 3b). After Termination I $U^{K'}_{37}$ SST increased slightly up to the core top value of 27.3°C.

[18] The TEX_{86} record at 74KL is again quite different from $U^{K'}_{37}$ SST record, but closely resembles the pattern evident in the TEX_{86} record from core NIOP905. TEX_{86} SST values for 74KL have a somewhat smaller range than in NIOP905 and vary between 24° and 30°C (Figure 3c). LGM SSTs for 74KL (~24°C) were slightly higher than at NIOP905 (~22.5°C). TEX_{86} SST values then rapidly increased to ~30°C between 18 and 16 cal kyr B.P. followed by a drop in SST down to 26°C between 16 and 14 cal kyr B.P. SST then rapidly increased again to 29°C at 12.5 cal kyr B.P. followed by a rapid drop to 27.5°C. SST then slowly decreased to the core top value of 26.4°C.

4. Discussion

4.1. Comparison of Core Tops and Present-Day SSTs

[19] One way of establishing the origin of the reconstructed SST of proxies is to compare core top reconstructed SSTs (0–2.5 cm depth representing the last ~300 years) with those of annual mean and seasonal mean SST (0–10 m depth). For NIOP905 the TEX_{86} and the $U^{K'}_{37}$ give a core top SSTs of 25.7 and 26.3°C, respectively. Considering the analytical error of 0.4°C and 0.2°C, respectively, these results correspond well with present-day annual mean SST of 26.0°C (Table 2). Similarly, at site 74KL both TEX_{86} and $U^{K'}_{37}$ SST, with core top values of 26.4°C and 27.3°C, respectively, correspond well with present-day annual mean SST of 26.8°C.

[20] Although both proxies seem to record annual mean SSTs, it has been reported that both Crenarchaeota [*Massana et al.*, 1998; *Murray et al.*, 1999; *Wuchter et al.*, 2005] and haptophyte algae [e.g., *Bac et al.*, 2003] vary considerably in abundance during the annual cycle. In the Arabian Sea primary production is strongly associated with upwelling dynamics and monsoonal cycles (Figure 1). This most likely determines the annual cycle of the abundance of organisms that produce the biomarkers on which the SST proxies are based. Trap studies in the coastal and central Arabian Sea show that more than 50% of the particle flux to the sediments occurs during the SW monsoon and to a lesser extent (~25%) during the NE monsoon [*Prahl et al.*, 2000; *Wakeham et al.*, 2002]. *Wakeham et al.* [2002] described a distinct succession in phytoplankton biomarker fluxes. During the early SW monsoon the biomarker flux is dominated by C_{30}-diol and C_{30}-ketols from *Proboscia*

diatoms [*Sinninghe Damsté et al.*, 2003]. This is followed by maximum fluxes of alkenones, and diatom and dinoflagellate sterols. At the end of the upwelling season the flux of 25:3 highly branched isoprenoid produced by *Rhizosolenoid* diatoms increase substantially. These findings are in good agreement with results from other sediment trap studies in central Arabian Sea area, where a sharp peak in the flux of alkenones was measured in the middle of the SW monsoon as well as a minor peak during the NE monsoon [*Prahl et al.*, 2000]. Taken together these studies indicate that sedimentary alkenones are mainly derived from alkenones produced during the SW monsoon and, to a lesser extent, during the NE monsoon. A recent study on the same sediment trap material from the *Wakeham et al.* [2002] in the Arabian Sea, showed that fluxes of GDGT material in a location near 74KL (Figure 1) were also highest during the SW monsoon and to a lesser degree in the NE monsoon (Wuchter et al., submitted manuscript, 2006). However, GDGT fluxes only moderately increased during both monsoon periods compared to the intermonsoon periods (approximately 3 times). In contrast, the fluxes of alkenones were substantially higher (approximately 9 times) during monsoon periods than in intermonsoon periods. Wuchter et al. (submitted manuscript, 2006) suggested that this is because the relative abundance of Crenarchaeota during upwelling is lower than outside the upwelling period, while the opposite is observed for phytoplankton abundance. This is in agreement with previous studies which showed a negative correlation between Crenarchaeota and phytoplankton abundance [*Massana et al.*, 1998; *Murray et al.*, 1999; *Wuchter et al.*, 2005]. On the basis of the above considerations, $U^{K'}_{37}$ SST values in the present-day Arabian Sea should correspond to the SST prevalent during the SW monsoon, while the crenarchaeotal TEX_{86} is also influenced by SST from periods outside the SW monsoon and thus perhaps reflects a more annual mean signal.

[21] On the basis of the sediment trap studies reported we can estimate the flux weighted annual SST for alkenones and GDGTs, i.e., the annual mean SST corrected for the times of the largest fluxes of these components, by combining alkenone and GDGT flux data from the central Arabian Sea [*Prahl et al.*, 2000; *Wakeham et al.*, 2002; Wuchter et al., submitted manuscript, 2006] and monthly average SST (Table 2). The flux weighted annual SST for alkenones is 1.4°C lower than $U^{K'}_{37}$ SST core top value for NIOP905 but only 0.8°C lower than core top $U^{K'}_{37}$ SST at 74KL (Table 2). The comparison of core top values to monthly mean SSTs (Table 2) suggests that the $U^{K'}_{37}$ is not recording the upwelling of cold water between June and September. During the SW monsoon, the Arabian Sea shows substantially lower SSTs, especially at NIOP905 where SSTs are up to 3°C lower than annual mean SST (Table 2). Hence it seems that the pulses in alkenone production during upwelling seasons do not have a substantial effect on the temperature signal recorded by $U^{K'}_{37}$ in the sediment. It should be noted, however, that most sediment trap studies cover just one cycle at one specific location and that interannual variability in production could be of importance [*Herbert*, 2003]. Furthermore, it is important to take into account that the core top (0–2.5 cm) represents an integrated SST signal of up to 300 years. Finally, the SST estimate from $U^{K'}_{37}$ analysis will also depend on the calibration used and can vary by up to 0.7°C (Table 2). However, other studies in the Arabian Sea show similar results, in that the flux of alkenones to the sediment is seasonal, yet an annual mean SST is recorded in the sediment core tops [*Doose-Rolinski et al.*, 2001; *Rosell-Melé et al.*, 2004]. A similar calculation for GDGT flux-weighted TEX_{86} SST yields 26.0°C and 26.8°C for NIOP905 and 74KL, respectively (Table 2). These values are identical to the actual annual mean SST and are within analytical error of the core top TEX_{86} value. The flux weighted TEX_{86} SST is higher than the flux-weighted $U^{K'}_{37}$ SST in agreement with the relatively higher fluxes of alkenones compared to GDGT during the SW monsoon. This suggests that the TEX_{86} is recording annual mean SST although, on the basis of the above considerations for the $U^{K'}_{37}$, we cannot exclude that certain seasonal periods may have a substantial influence on the TEX_{86}.

[22] We can thus not rule out that there is a seasonal component in our SST proxies, even though this is not apparent from our core top results. It is also possible that the seasonal signal was stronger during certain periods of time, e.g., during the LGM, which may explain why the proxies show different behavior in our sedimentary record (see section 4.2).

4.2. Comparison of SST Proxy Records

[23] The $U^{K'}_{37}$ records of the two cores differ in both timing and magnitude of SST variations during deglaciation but both record relatively small variations in SST of <3°C. Remarkably, $U^{K'}_{37}$ SSTs reconstructed for the LGM for both sites are very similar at 25°C but the rise in SST during Termination I was much larger at 74 KL (2°C) than at NIOP905 (0.5°C). This is in agreement with previous results of *Sonzogni et al.* [1998] who showed that the $U^{K'}_{37}$ SST rising during Termination I is only 0.3°C for NIOP 905 but 1°–3°C at other sites in the Indian Ocean. The reasons for the different $U^{K'}_{37}$ records of the two sites are unclear but based on the study of *Sonzogni et al.* [1998] the unusual $U^{K'}_{37}$ record at NIOP905 seems to be a local feature. After Termination I, $U^{K'}_{37}$ SST in both records vary by <1°C suggesting relatively stable conditions. Remarkably, the $U^{K'}_{37}$ record at 74KL is roughly similar in phase to changes in $\delta^{18}O$ record, which contains a substantial SST component, in contrast to the $U^{K'}_{37}$ record at NIOP905 which is dissimilar to the $\delta^{18}O$ record. However, it should be noted that comparison of $U^{K'}_{37}$ record and $\delta^{18}O$ record should be done with caution as SST is not the only factor determining $\delta^{18}O$ (e.g., $\delta^{18}O$ of seawater, salinity) and, despite being analyzed in the same sediment layer, could represent SST of different ages [cf. *Ohkouchi et al.*, 2002]

[24] Both 74KL and NIOP905 cores gave similar TEX_{86} SST records, taking into account the errors in TEX_{86} analysis and the age models. However, they are quite different from the $U^{K'}_{37}$ records at both sites and show substantially larger variability in SST. For example, SSTs rose by 4°–6°C during Termination I with a pronounced cooling between 15.5 and 12 cal kyr B.P. while $U^{K'}_{37}$ SST rose fairly smoothly by only 0.5°–1.5°C. The trends in the

TEX_{86} SST records are also different from those in $\delta^{18}O$ records; for example, the $\delta^{18}O$ records show a more gradual trend from LGM to Holocene and no pronounced cooling between 15.5 and 12 cal kyr B.P. However, comparison between the TEX_{86} record and $\delta^{18}O$ record are hampered by the same problems as discussed for the $U^{K'}_{37}$ record and $\delta^{18}O$ record. In contrast, the differences between the two organic SST proxy records, TEX_{86} and $U^{K'}_{37}$, are unlikely to be caused by seawater composition changes and are more likely to be caused by the different response of the proxy-producing organisms to changes in climatic conditions such as monsoon and upwelling intensity, as has been documented for this area [e.g., *Ivanochko*, 2005]. Thus both proxies probably do not record annual mean SST but are strongly influenced by seasonal SSTs. Below we attempt to explain the impact of this component on LGM SST reconstruction, and the phasing of SST changes.

4.3. LGM SST Reconstructions

[25] Large discrepancies exist in estimates of tropical LGM temperatures [*Mix et al.*, 2001]. These discrepancies are dependent on the method used to estimate LGM temperatures. Transfer function values of distributions of planktic foraminifera show small SST changes for the glacial-interglacial transition; for example, the CLIMAP project reconstruction suggests SSTs of 2°C lower for the LGM in the Arabian Sea [*CLIMAP Project Members*, 1981]. *Mix et al.* [2001] suggested that CLIMAP might have underestimated ice age cooling in the tropics, and that SST could have cooled almost 3°C. $U^{K'}_{37}$ studies in the Arabian Sea and Indian Ocean show differences between the LGM and present-day SST of 1.5 to 2.5°C [*Bard et al.*, 1997; *Sonzogni et al.*, 1998; *Schulte and Müller*, 2001; *Rosell-Melé et al.*, 2004]. Analyses of Mg/Ca ratios of planktic foraminifera at tropical areas in the equatorial Atlantic and Pacific show a 2.5°–3°C cooler SST during the LGM [*Hastings et al.*, 1998; *Lea et al.*, 2000] while a recent summary suggested 2°–3.5°C lower SSTs in tropical areas during the LGM [*Barker et al.*, 2005, and references therein]. Sr/Ca ratios in corals indicate up to 5°C difference in SST between the LGM and the present [*Guilderson et al.*, 1994]. Reconstructions of SST in the western Arabian Sea using artificial neural networks based on quantitative analysis of planktonic foraminifera suggests LGM SST 2°C below Holocene values [*Naidu and Malmgren*, 2005], in agreement with predictions based on atmosphere-ocean models [*Mix et al.*, 2001, and references therein]. Some modeling results also suggest relatively cool temperatures in the tropics with LGM SST values approximately 4°C lower than Holocene SST values for the Arabian Sea [*Toracinta et al.*, 2004]. In general, proxy data suggest LGM SSTs between 1.5° and 5°C lower than present-day values, suggesting that Arabian Sea LGM temperatures were between 21.5° and 24.5°C.

[26] The proxy records in this study also reveal a difference, i.e., SSTs estimated for the LGM are ~23°C with TEX_{86} and ~25°C with the $U^{K'}_{37}$. Thus the temperature increase from the LGM to present day is 0.5°–1.5°C when measured with $U^{K'}_{37}$, and 3°–4°C when we use the TEX_{86}. The LGM SST values reconstructed with TEX_{86} are slightly lower than other LGM estimates (see above). However, LGM SST TEX_{86} estimates are still well within the range measured by other proxies in the tropical area. Furthermore, preliminary measurements of Mg/Ca ratio of planktic foraminifera in the NIOP905 core suggest that calcification temperatures were up to 3°C lower during the LGM compared to the late Holocene (P. Anand et al., personal communication, 2004). This is in good agreement with the TEX_{86} proxy estimates of glacial-interglacial SST changes in the Arabian Sea.

[27] On the other hand, $U^{K'}_{37}$ SSTs in both cores indicate that the LGM was only 0.5°–1.5°C cooler than present day and suggest LGM SSTs of 25°C. These temperatures are somewhat higher than SST estimates based on inorganic proxies and the TEX_{86}. Several studies show that in general alkenone-based SSTs give smaller changes from the LGM to the Holocene in tropical and subtropical areas compared to other proxies such as Sr/Ca or $\delta^{18}O$ [*Rosell-Melé et al.*, 2004; *Toracinta et al.*, 2004] for reasons which are presently unclear. Thus it seems that the LGM TEX_{86} SST estimates are somewhat lower than estimates using other proxies and modeling results while our $U^{K'}_{37}$ LGM SST estimates are somewhat higher.

[28] The strong control of primary production in the area by upwelling may explain why alkenone-based glacial SSTs are substantially higher than those based on the TEX_{86}. A decrease in the upwelling intensity has been documented for the Arabian Sea during the LGM [e.g., *Naidu and Malmgren*, 2005] and the Ba/Al record from NIOP905, a measure for marine productivity, shows lower ratios during the LGM and at the beginning of Termination I [*Ivanochko et al.*, 2005] suggesting lower productivity. It is reasonable to assume that these large changes could affect the seasonal abundance of the organisms living in the upwelling region. A decrease in the intensity of the SW monsoon during the LGM would indeed affect the depth of alkenone production, increase the stratification of surface waters and reduce production. All those changes would affect the alkenone temperature signal [*Mix et al.*, 2000, *Prahl et al.*, 2003] and could, likewise, affect the production and flux of crenarchaeotal GDGTs during the annual cycle. It has been suggested that the monsoon dynamics might have been different during the LGM with a very weak SW monsoon and relatively strong NE monsoon resulting in a shift in alkenone production to the winter months in the Arabian Sea [*Higginson et al.*, 2004]. This would result in relatively higher SSTs during the LGM as temperatures during the SW monsoon are lower than during the NE monsoon (Table 2). The idea of a seasonal shift in alkenone production has indeed been used to explain the relatively warm glacial SST measured by $U^{K'}_{37}$ in the subtropical North Atlantic [*Chapman et al.*, 1996]. If this also occurred at our study sites then the $U^{K'}_{37}$ glacial SSTs values may be reflecting preferentially NE monsoon SST during the LGM. This is in contrast to the present-day situation in which the alkenones seem to record annual mean temperature. Possibly, such changes in monsoon strength were of lesser importance for the TEX_{86} SST record as the seasonal abundance of Crenarchaeota is probably not so tied to upwelling dynamics and the relative GDGT flux increase during monsoon

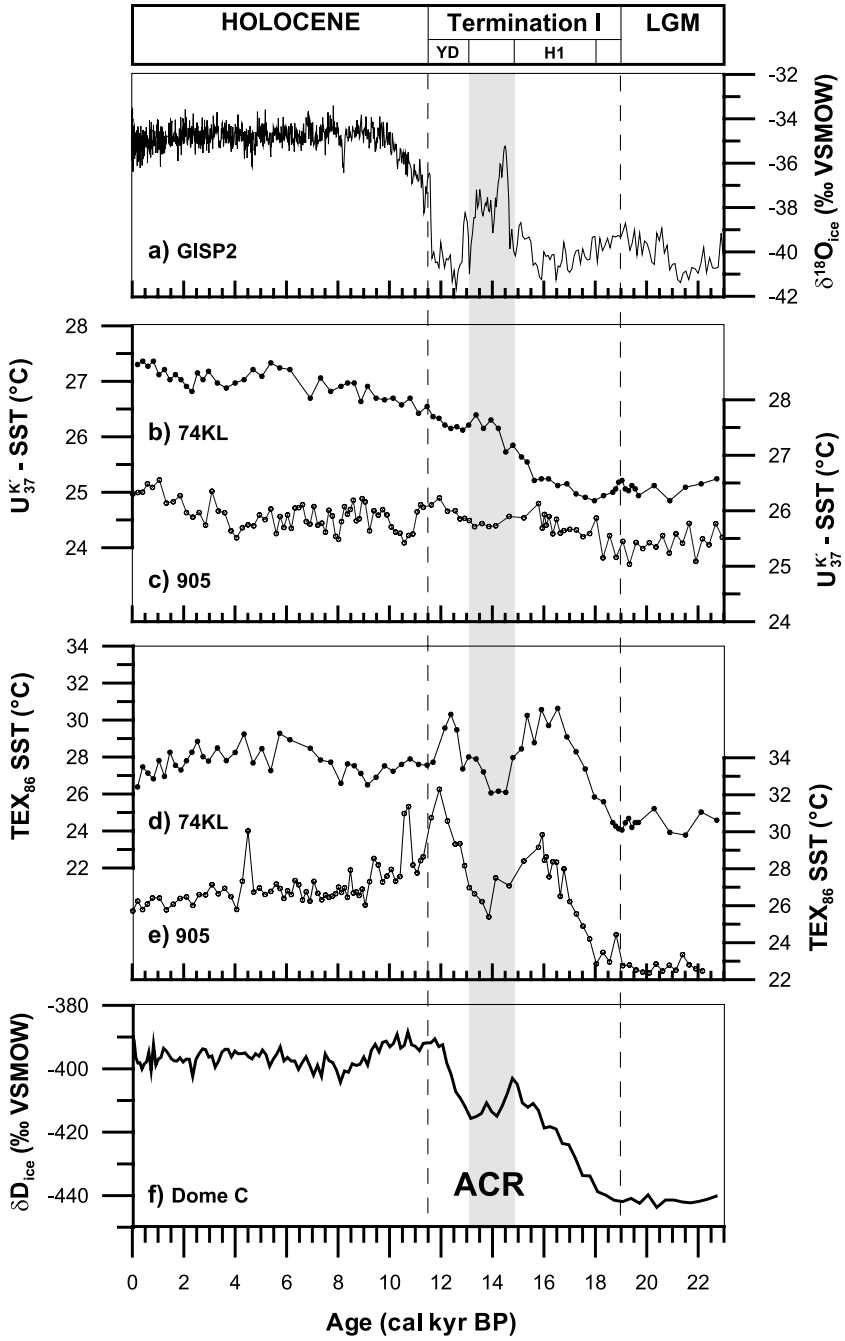

Figure 4. Comparison of SST records from the western Arabian Sea with ice core isotope records from Greenland and the Antarctic: (a) Greenland Ice Sheet Project 2 (GISP2) $\delta^{18}O$ record from Greenland [*Dansgaard et al.*, 1993], (b) $U^{K'}_{37}$ SST for 74KL, (c) $U^{K'}_{37}$ SST for NIOP905, (d) TEX_{86} SST from 74KL, (e) TEX_{86} SST from NIOP905, and (f) δD from Dome C in Antarctica [*Jouzel et al.*, 2003]. ACR indicates the Antarctic cold reversal.

periods is lower than for the alkenones (C. Wuchter et al., submitted manuscript, 2006). Alternatively, the location of strong upwelling sites, such as those at NIOP905 and 74KL, may have shifted through changes in ocean circulation during the last 23 kyr and in this way have affected the dynamics of the organic proxies.

4.4. Phasing of SST Records During Termination I

[29] Comparison of the TEX_{86} SST records with ice core records reflecting temperature from Antarctica (δD EPICA Dome C, Figure 4f) [*Jouzel et al.*, 2003] and Greenland ($\delta^{18}O$ GISP2, Figure 4a) [*Dansgaard et al.*, 1993] shows that the increase in TEX_{86} SST from the LGM to the Early

Holocene is in phase with the Southern Hemisphere warming, suggesting that this proxy is primarily forced by Southern Hemisphere climate change (Figure 4). The TEX_{86} SST records also show a cooling during Termination I in phase with the Antarctic cold reversal, which has been noted exclusively in the Southern Hemisphere [*Stenni et al.*, 2001] (Figure 4). The $U^{K'}_{37}$ SSTs at 74KL lag Antarctic records and resemble more the Arctic ice record (Figure 4) while $U^{K'}_{37}$ SST record at NIOP905 does not show much variation at all and perhaps only slightly resembles the Antarctica record (Figure 4). In addition, the $U^{K'}_{37}$ SST record at 74KL shows a small drop in SST in phase with the Younger Dryas in the Northern Hemisphere. Previous studies in the Arabian Sea area show that the $U^{K'}_{37}$ records from the Oman and Pakistan Margins are also predominantly affected by Northern Hemisphere climate dynamics [*Schulte and Müller*, 2001; *Doose-Rolinski et al.*, 2001; *Higginson et al.*, 2004]. The reason why the $U^{K'}_{37}$ SST record at NIOP905 is not reflecting Northern Hemisphere dynamics is unclear. It should be noted that the NIOP 905 $U^{K'}_{37}$ record is very different from other $U^{K'}_{37}$ records in the area [*Sonzogni et al.*, 1998], suggesting that local features may have overwritten the global change in SST.

[30] The question thus remains why we detect Southern Hemisphere dynamics with the TEX_{86} proxy, even at 74KL, and not with the $U^{K'}_{37}$ proxy. This may only be explained if the TEX_{86} proxy is more influenced by the SW monsoon, when the Southern Hemisphere dynamics dominate the area, even when this was substantially reduced during the LGM and Termination I. In contrast, the $U^{K'}_{37}$ may be more influenced by the NE monsoon during this time, as suggested previously [*Higginson et al.*, 2004] and therefore records Northern Hemisphere climate. To the best of our knowledge SST records of tropical oceans have not revealed, until now, a dominant Southern Hemisphere component making it difficult to speculate what the mechanism behind the control on the TEX_{86} SST is.

4.5. Holocene SST Reconstructions

[31] Similar to the ice core records no large short-term changes in SST are observed during the Late Holocene in neither the TEX_{86} nor the $U^{K'}_{37}$ SST records. However, both TEX_{86} and $U^{K'}_{37}$ values for NIOP905 and 74KL show relatively consistent opposing SST trends during the Holocene. While the TEX_{86} values show a slight decrease in SST from Termination I to present-day values, the $U^{K'}_{37}$ record indicates a small increase in SST in this time period. Using artificial neural networks analysis of the distributions of planktic foraminifera, *Naidu and Malmgren* [2005] show a cooling trend in the Arabian Sea in the Holocene, which is more pronounced in boreal winter than in boreal summer. This cooling trend is also observed in the western Pacific, eastern Atlantic and western Mediterranean as well as in the Arabian Sea [*Naidu and Malmgren*, 2005, and references therein]. In contrast, $U^{K'}_{37}$ SST records over the last 7 kyr have shown a general warming in the tropics [*Kim et al.*, 2004]. A data-model comparison study based on globally distributed $U^{K'}_{37}$ SST records and transient ensemble climate simulations suggests that the Holocene warming in the tropics is due to an orbitally driven insolation increase during the boreal winter (December-January-February) in the low latitudes [*Lorenz et al.*, 2006]. The apparent discrepancy between TEX_{86} SST records and $U^{K'}_{37}$ SST records is most likely caused by the fact that SST proxies are not consistently recording annual mean SST but seasonal SST.

5. Conclusions

[32] $U^{K'}_{37}$ and TEX_{86} SST records from two sites in the Arabian Sea revealed different temperature variations over the last 23 kyr for each proxy. TEX_{86} SST records were similar at two sampling sites in the Arabian Sea over the last glacial-interglacial cycle and they are in phase with temperature changes recorded in Antarctica ice core records. This suggests that the TEX_{86} records of SST in the area are mainly controlled by the Southern Hemisphere climate dynamics during the SW monsoon. $U^{K'}_{37}$ SST records from the same cores are different in magnitude of change and differ also in phase, and are party in phase with Northern Hemisphere climate dynamics during the NE monsoon. This is likely due to different growing seasons of the biomarker source organisms, and to a change in the upwelling dynamics and monsoon strengths between the LGM and the Holocene. Our results suggest that if the impact of seasonality on the different organic proxies can be better constrained, then complementary information on SST can be obtained by this multiproxy approach.

[33] **Acknowledgments.** We would like to thank Martijn Woltering and Annemiek Vos van Avezaathe for analytical support; Lydie Herfort and Gert Jan Reichart for useful comments; Ellen Hopmans for assistance with the HPLC/MS; Tjeerd van Weering, Erica Koning, and Geert Jan Brummer for providing access to the NIOP905 core; and Frank Sirocko for the 74KL sediment samples. Andreas Lückge, Joe Werne, and two anonymous reviewers are thanked for constructive comments on earlier drafts of this paper. This project was supported by NWO-ALW (project 152911) and by the EU project 6C (contract EVK2-2001-00179-6C).

References

Andruleit, H. A., U. Von Rad, A. Bruns, and V. Ittekkot (2000), Coccolithophore fluxes from sediment traps in the northeastern Arabian Sea off Pakistan, *Mar. Micropaleontol.*, *38*, 285–308.

Bac, M. G., K. R. Buck, F. P. Chavez, and S. C. Brassell (2003), Seasonal variation in alkenones, bulk suspended POM, plankton and temperature in Monterey Bay, California: Implications for carbon cycling and climate assessment, *Org. Geochem.*, *34*, 837–855.

Bard, E., F. Rostek, and C. Sonzogni (1997), Interhemispheric synchrony of the last deglaciation inferred from alkenone palaeothermometry, *Nature*, *385*, 707–710.

Barker, S., I. Cacho, H. Benway, and K. Tachikawa (2005), Planktonic foraminiferal Mg/Ca as a proxy for past oceanic temperatures: A methodological overview and data compilation for the Last Glacial Maximum, *Quat. Sci. Rev.*, *24*, 821–834.

Brassell, S. C., G. Eglinton, I. T. Marlowe, U. Pflaumann, and M. Sarnthein (1986), Molecular stratigraphy: A new tool for climatic assessment, *Nature*, *320*, 129–133.

Bush, A. B. G. (2002), A comparison of simulated monsoon circulations and snow accumu-

lation in Asia during the mid-Holocene and at the Last Glacial Maximum, *Global Planet. Change*, *32*, 331–347.

Chapman, M. R., N. J. Shackleton, M. Zhao, and G. Eglinton (1996), Faunal and alkenone reconstructions of subtropical North Atlantic surface hydrography and paleotemperature over the last 28 kyr, *Paleoceanography*, *11*, 343–357.

Chave, K. E. (1954), Aspects of the biogeochemistry of magnesium. 1. Calcareous marine organisms, *J. Geol.*, *62*, 266–283.

CLIMAP Project Members (1981), Seasonal reconstructions of the Earth's surface at the Last Glacial Maximum, *Geol. Soc. Am. Map Chart Ser.*, *MC-36*.

Dansgaard, W., et al. (1993), Evidence for general instability of past climate from a 250-Kyr ice-core record, *Nature*, *364*, 218–220.

Doose-Rolinski, H., U. Rogalla, G. Scheeder, A. Lückge, and U. Von Rad (2001), High-resolution temperature and evaporation changes during the late Holocene in the northeastern Arabian Sea, *Paleoceanography*, *16*, 358–367.

Elderfield, H., and G. Ganssen (2000), Past temperature and $\delta^{18}O$ of surface ocean waters inferred from foraminiferal Mg/Ca ratios, *Nature*, *405*, 442–445.

Emiliani, C. (1955), Pleistocene temperatures, *J. Geol*, *63*, 538–578.

Grootes, P. M., and M. Stuiver (1997), Oxygen 18/16 variability in Greenland snow and ice with 10^3- to 10^5-year time resolution, *J. Geophys. Res.*, *102*, 26,455–26,470.

Guilderson, T. P., R. G. Fairbanks, and J. L. Rubenstone (1994), Tropical temperature variations since 20,000 years ago: Modulating interhemispheric climate change, *Science*, *263*, 663–665.

Hastings, D. W., A. D. Russell, and S. R. Emerson (1998), Foraminiferal magnesium in Globeriginoides sacculifer as a paleotemperature proxy, *Paleoceanography*, *13*, 161–169.

Herbert, T. D. (2003), Alkenone paleotemperature determinations, in *Treatise on Geochemistry*, vol. 6, *The Ocean and Marine Geochemistry*, edited by H. D. Holland and K. K. Turekian, pp. 391–432, Elsevier, New York.

Higginson, M. J., M. A. Altabet, L. Wincze, T. D. Herbert, and D. W. Murray (2004), A solar (irradiance), trigger for millennial-scale abrupt changes in the southwest monsoon?, *Paleoceanography*, *19*, PA3015, doi:10.1029/2004PA001031.

Hoefs, M. J. L., S. Schouten, J. W. de Leeuw, L. L. King, S. G. Wakeham, and J. S. Sinninghe Damsté (1997), Ether lipids of planktonic archaea in the marine water column, *Appl. Environ. Microbiol.*, *63*, 3090–3095.

Hopmans, E. C., S. Schouten, R. D. Pancost, M. T. J. Van der Meer, and J. S. Sinninghe Damsté (2000), Analysis of intact tetraether lipids in archaeal cell material and sediments by high performance liquid chromatography/atmospheric pressure chemical ionization mass spectrometry, *Rapid Comm. Mass Spectrom.*, *14*, 585–589.

Hopmans, E. C., J. W. H. Weijers, E. Schefuss, L. Herfort, J. S. S. Damste, and S. Schouten (2004), A novel proxy for terrestrial organic matter in sediments based on branched and isoprenoid tetraether lipids, *Earth Planet. Sci. Lett.*, *224*, 107–116.

Ivanochko, T. S. (2005), Sub-orbital scale variations in the intensity of the Arabian Sea monsoon, Ph.D. thesis, 230 pp., Univ. of Edinburgh, Edinburgh.

Ivanochko, T. S., R. S. Ganesham, G. J. Brummer, G. Ganssen, S. J. A. Jung, S. G. Moreton, and D. Kroon (2005), Variations in tropical convection as an amplifier of global climate change at the millennial scale, *Earth Planet. Sci. Lett.*, *235*, 302–314.

Ivanova, E. (1999), Late Quaternary monsoon history and paleoproductivity of the western Arabian Sea, Ph.D. thesis, 172 pp., Free Univ., Amsterdam.

Jouzel, J., F. Vimeux, N. Caillon, G. Delaygue, G. Hoffmann, V. Masson-Delmotte, and F. Parrenin (2003), Magnitude of isotope/temperature scaling for interpretation of central Antarctic ice cores, *J. Geophys. Res.*, *108*(D12), 4361, doi:10.1029/2002JD002677.

Jung, S. J. A., G. M. Ganssen, and G. R. Davies (2001), Multidecadal variation in the early Holocene outflow of Red Sea water into the Arabian Sea, *Paleoceanography*, *16*, 658–668.

Jung, S. J. A., G. R. Davies, G. Ganssen, and D. Kroon (2002), Decadal-centennial scale monsoon variations in the Arabian Sea during the early Holocene, *Geochem. Geophys. Geosyst.*, *3*(10), 1060, doi:10.1029/2002GC000348.

Karner, M. B., E. F. DeLong, and D. M. Karl (2001), Archaeal dominance in the mesopelagic zone of the Pacific Ocean, *Nature*, *409*, 507–510.

Kim, J.-H., R. R. Schneider, P. J. Müller, and G. Wefer (2002), Interhemispheric comparison of deglacial sea-surface temperature patterns in Atlantic eastern boundary currents, *Earth Planet. Sci. Lett.*, *194*, 383–393.

Kim, J.-H., N. Rimbu, S. J. Lorenz, G. Lohmann, S. I. Nam, S. Schouten, C. Ruhlemann, and R. R. Schneider (2004), North Pacific and North Atlantic sea-surface temperature variability during the Holocene, *Quat Sci. Rev.*, *23*, 2141–2154.

Konekes, M., A. E. Bernhard, J. R. de la Torre, C. B. Walker, J. B. Waterbury, and D. A. Stahl (2005), Isolation of an autotrophic ammonia-oxidizing marine archaeon, *Nature*, *237*, 543–546.

Lea, D. W. (2003), Elemental and isotopic proxies of past ocean temperatures, in *Treatise on Geochemistry*, vol. 6, *The Ocean and Marine Geochemistry*, edited by H. D. Holland and K. K. Turekian, pp. 365–390, Elsevier, New York.

Lea, D. W., D. K. Pak, and H. J. Spero (2000), Climate impact of late Quaternary equatorial Pacific sea surface temperature variations, *Science*, *289*, 1719–1724.

Levitus, S., and T. P. Boyer (1994), *World Ocean Atlas 1994*, vol. 4, *Temperature*, *NOAA ATLAS NESDIS*, vol. 4, 117 pp., NOAA, Silver Spring, Md.

Lorenz, J. S., J. H. Kim, N. Rimbu, R. R. Schneider, and G. Lohmann (2006), Orbitally driven insolation forcing on Holocene climate trends: Evidence from alkenone data and climate modeling, *Paleoceanography*, *21*, PA1002, doi:10.1029/2005PA001152.

Massana, R., L. T. Taylor, A. E. Murray, K. Y. Wu, W. H. Jeffrey, and E. F. DeLong (1998), Vertical distribution and temporal variation of marine planktonic archaea in the Gerlache Strait, Antarctica, during early spring, *Limnol. Oceanogr.*, *43*, 607–617.

Massana, R., E. F. DeLong, and C. Pedrós-Alió (2000), A few cosmopolitan phylotypes dominate planktonic archaeal assemblages in widely different oceanic provinces, *Appl. Environ. Microbiol.*, *66*, 1777–1787.

Mix, A. C., E. Bard, G. Eglinton, L. D. Keigwin, A. C. Ravelo, and Y. Rosenthal (2000), Alkenones and multiproxy strategies in paleoceanographic studies, *Geochem. Geophys. Geosyst.*, *1*(11), doi:10.1029/2000GC000056.

Mix, A. C., E. Bard, and R. Schneider (2001), Environmental processes of the ice age: Land, oceans, glaciers (EPILOG), *Quat. Sci. Rev.*, *20*, 627–657.

Müller, P., G. Kirst, G. Ruhland, I. von Storch, and A. Rosell-Melé (1998), Calibration of the alkenone paleotemperature index $U^{K'}_{37}$ based on core-tops from the eastern South Atlantic and the global ocean (60°N–60°S), *Geochim. Cosmochim. Acta*, *62*, 1757–1772.

Murray, A. E., A. Blakis, R. Massana, S. Strawzewski, U. Passow, A. Alldredge, and E. F. DeLong (1999), A time series assessment of planktonic archaeal variability in the Santa Barbara Channel, *Aquat. Microbiol. Ecol.*, *20*, 129–145.

Naidu, P. D., and B. A. Malmgren (2005), Seasonal sea surface temperature contrast between the Holocene and last glacial period in the western Arabian Sea (Ocean Drilling Project Site 723A): Modulated by monsoon upwelling, *Paleoceanography*, *20*, PA1004, doi:10.1029/2004PA001078.

Nurnberg, D., J. Bijma, and C. Hemleben (1996), Assessing the reliability of magnesium in foraminiferal calcite as a proxy for water mass temperatures, *Geochim. Cosmochim. Acta*, *60*, 803–814.

Ohkouchi, N., T. I. Eglinton, L. D. Keigwin, and J. M. Hayes (2002), Spatial and temporal offsets between proxy records in a sediment drift, *Science*, *298*, 1224–1227.

Powers, L. A., T. C. Johnson, J. P. Werne, I. S. Castañeda, E. Hopmans, J. S. Sinninghe Damsté, and S. Schouten (2005), Large temperature variability in the southern African tropics since the Last Glacial Maximum, *Geophys. Res. Lett.*, *32*, L08706, doi:10.1029/2004GL022014.

Prahl, F. G., and S. G. Wakeham (1987), Calibration of unsaturation patterns in long-chain ketone compositions for paleotemperature assessment, *Nature*, *330*, 367–369.

Prahl, F. G., L. A. Muehlhausen, and D. L. Zahnle (1988), Further evaluation of long-chain alkenones as indicators of paleoceanographic conditions, *Geochim. Cosmochim. Acta*, *52*, 2303–2310.

Prahl, F. G., J. Dymond, and M. A. Sparrow (2000), Annual biomarker record for export production in the central Arabian Sea, *Deep Sea Res., Part II*, *47*, 1581–1604.

Prahl, F. G., G. V. Wolfe, and M. A. Sparrow (2003), Physiological impacts on alkenone paleothermometry, *Paleoceanography*, *18*(2), 1025, doi:10.1029/2002PA000803.

Rixen, T., V. Ittekkot, B. Haake-Gaye, and P. Schäfer (2000), The influence of the SW monsoon on the deep-sea organic carbon cycle in the Holocene, *Deep Sea Res., Part II*, *47*, 2629–2651.

Rosell-Melé, A., E. Bard, K. C. Emeis, B. Grieger, C. Hewitt, P. J. Müller, and R. R. Schneider (2004), Sea surface temperature anomalies in the oceans at the LGM estimated from the alkenone-$U^{K'}_{37}$ index: Comparison with GCMs, *Geophys. Res. Lett.*, *31*, L03208, doi:10.1029/2003GL018151.

Schouten, S., E. C. Hopmans, E. Schefuss, and J. S. Sinninghe Damsté (2002), Distributional variations in marine crenarchaeotal membrane lipids: A new tool for reconstructing ancient sea water temperatures?, *Earth Planet. Sci. Lett.*, *204*, 265–274.

Schouten, S., E. C. Hopmans, and J. S. Sinninghe Damsté (2004), The effect of maturity and depositional redox conditions on archaeal tetraether lipid paleothermometry, *Org. Geochem.*, *35*, 567–571.

Schulte, S., and P. J. Müller (2001), Variations of sea surface temperature and primary productivity during Heinrich and Dansgaard-Oescher events in the northeastern Arabian Sea, *Geo Mar. Lett.*, *21*, 168–175.

Schulz, H., U. von Rad, and H. Erlenkeuser (1998), Correlation between Arabian Sea and Greenland climate oscillations of the past 110,000 years, *Nature*, *393*, 54–57.

Sinninghe Damsté, J. S., S. Rampen, W. I. C. Rijpstra, B. Abbas, G. Muyzer, and S. Schouten (2003), A diatomaceous origin for long-chain diols and mid-chain hydroxy methyl alkanoates widely occurring in Quaternary marine sediments: Indicators for high-nutrient conditions, *Geochim. Cosmochim. Acta*, *67*, 1339–1348.

Sirocko, F., M. Sarnthein, H. Erlenkeuser, H. Lange, M. Arnold, and J. C. Duplessy (1993), Century-scale events in monsoonal climate over the past 24,000 years, *Nature*, *364*, 322–324.

Sonzogni, C., E. Bard, F. Rostek, R. Lafont, A. Rosell-Melé, and G. Eglinton (1997), Core-top calibration of the alkenone index vs sea surface temperature in the Indian Ocean, *Deep Sea Res., Part II*, *44*, 1445–1460.

Sonzogni, C., E. Bard, and F. Rostek (1998), Tropical sea-surface temperature during the last glacial period: A view based on alkenones in Indian Ocean sediments, *Quat. Sci. Rev.*, *17*, 1185–1201.

Southon, J., M. Kashgarian, M. Fontugne, B. Metivier, and W. W. S. Yim (2002), Marine reservoir corrections for the Indian Ocean and southeast Asia, *Radiocarbon*, *44*, 167–180.

Spero, H. J., J. Bijma, D. W. Lea, and B. E. Bemis (1997), Effect of seawater carbonate concentration on foraminiferal carbon and oxygen isotopes, *Nature*, *390*, 497–500.

Staubwasser, M., F. Sirocko, P. M. Grootes, and H. Erlenkeuser (2002), South Asian monsoon climate change and radiocarbon in the Arabian Sea during early and mid Holocene, *Paleoceanography*, *17*(4), 1063, doi:10.1029/2000PA000608.

Stenni, B., V. Masson-Delmotte, S. Johnsen, J. Jouzel, A. Longinelli, E. Monnin, R. Röthlisberger, and E. Selmo (2001), An oceanic cold reversal during the last deglaciation, *Science*, *293*, 2074–2077.

Toracinta, E. R., R. J. Oglesby, and D. H. Bromwich (2004), Atmospheric response to modified CLIMAP ocean boundary conditions during the Last Glacial Maximum, *J. Clim.*, *17*, 504–522.

Wakeham, S. G., M. L. Peterson, J. I. Hedges, and C. Lee (2002), Lipid biomarker fluxes in the Arabian Sea: With a comparison to the equatorial Pacific Ocean, *Deep Sea Res., Part II*, *49*, 2265–2301.

Wang, Y. J., H. Cheng, R. L. Edwards, Z. S. An, J. Y. Wu, C. C. Shen, and J. A. Dorale (2001), A high-resolution absolute-dated late Pleistocene monsoon record from Hulu Cave, China, *Science*, *294*, 2345–2348.

Wefer, G., W. H. Berger, J. Bijma, and G. Fisher (1999), Clues to ocean history: A brief overview of proxies, in *The Use of Proxies in Palaeoceanography: Examples From the South Atlantic*, edited by G. Fisher and G. Wefer, pp. 1–68, Springer, New York.

Weijers, J., W. H. S. Schouten, M. van den Linden, B. van Geel, and J. S. Sinninghe Damsté (2004), Water table related variations in the abundance of intact archaeal membrane lipids in a Swedish peat bog, *FEMS Microbiol. Lett.*, *239*, 51–56.

World Ocean Atlas (1998), Internal report 16, http://www.nodc.noaa.gov/OC5/SELECT/dbsearch/dbsearch.html, Natl. Oceanogr. Data Cent., Silver Spring, Md.

Wuchter, C., S. Schouten, M. J. L. Coolen, and J. S. Sinninghe Damsté (2004), Temperature-dependent variation in the distribution of tetraether membrane lipids of marine Crenarchaeota: Implications for TEX_{86} paleothermometry, *Paleoceanography*, *19*, PA4028, doi:10.1029/2004PA001041.

Wuchter, C., S. Schouten, S. G. Wakeham, and J. S. Sinninghe Damsté (2005), Temporal and spatial variation in tetraether membrane lipids of marine Crenarchaeota in particulate organic matter: Implications for TEX_{86} paleothermometry, *Paleoceanography*, *20*, PA3013, doi:10.1029/2004PA001110.

C. Huguet, S. Schouten, and J. S. Sinninghe Damsté, Department of Marine Biogeochemistry and Toxicology, Royal Netherlands Institute for Sea Research (NIOZ), P.O. Box 59, NL-1790AB Den Burg, Texel, Netherlands. (huguet@nioz.nl)

J.-H. Kim, Centre de Formation et de Recherche sur l'Environnement Marin (CEFREM)-CNRS UMR 5110, Université de Perpignan, 52 avenue Paul Alduy, 66860 Perpignan Cedex, France.